Micropatterning a Chemotactic Gradient in a Cell-laden Hydrogel to Direct Cell Migration

---

A

Thesis

Presented to

the faculty of the School of Engineering and Applied Science

University of Virginia

---

in partial fulfillment

of the requirements for the degree

Master of Science

by

Steven Tate

May 2023

APPROVAL SHEET

This

Thesis

Master of Science

Author: Steven Tate

This Thesis has been read and approved by the examing committee:

Advisor: Dr. Nathan Swami

Advisor:

Committee Member: Dr. Harry Powell, Jr.

Committee Member: Dr. Christopher Highley

Committee Member:

Committee Member:

Committee Member:

Committee Member:

Accepted for the School of Engineering and Applied Science:

Jennifer L. West, School of Engineering and Applied Science

May 2023

Micropatterning a Chemotactic Gradient in a Cell-laden Hydrogel to Direct Cell Migration

Abstract

Microfluidic systems enable the creation of highly controlled chemical gradients through modulated flow and diffusional profiles to spatially direct cell migration events. These are usually conducted in closed systems; wherein accurate flow control is possible. However, for *in vitro* 3D culture systems, cells must be cultured in millimeter-scale hydrogel slabs to recapitulate the cell microenvironment, which is difficult to support in a closed microfluidic system. Open microfluidic systems can ameliorate this problem. But flow control in an open system is much harder to achieve. A tailor-made hydrogel can be patterned at the millimeter scale and integrated with a fluidic system to study cellular responses to a chemotactic gradient. Combining such a system with live-cell imaging would allow for the spatiotemporal quantification of the chemical gradient and the cellular reaction. Here, we present the design, patterning, and integration techniques to create a cell-laden hydrogel in an open-top culture. Bounded by adjoining open microfluidic channels, the system generates a chemotactic gradient to direct U87 glioma cell migration. The hydrogel is fabricated through a positive-negative-positive process with a positive 3D-printed mold, negative polydimethylsiloxane (PDMS) mold, and photo-crosslinking of the hydrogel structure. The composite hydrogel is composed of gelatin methacrylate (GelMA) and hyaluronic acid (HA) to mimic the properties of brain tissue. Stromal-derived factor 1 (SDF-1), or CXCL12, will be utilized as the chemoattractant for gradient generation across a specific section of the hydrogel. Fluorescence and brightfield imaging will be employed to quantify cellular migration and signaling.

Table of Contents

List of Figures and Tables:

Chapter 1: Introduction

Microfluidics

Microfluidics is both a science and technology that refers to the manipulation of picolitres to microliters within confined channels[1]. Over years of research and development, microfluidics and "lab-on-chip" devices have become popular for their use in diagnostic and point-of-care applications[2]. These devices are particularly effective in directing fluid flow in an extremely predictable and controlled manner. By changing device parameters, fluid flow can be treated as laminar. This greatly reduces the complexity of flow calculations when involving chemical reactions, diffusion patterns, and particle transport. Keeping a low Reynold's number (Re), shown in equation (1) where ρ is the density of the fluid, v is the flow velocity, L is the characteristic linear dimension, and μ is the dynamic viscosity of the fluid[3].

$$Re = \frac{\rho v L}{\mu} \qquad (1)$$

This relationship is important in both closed and open microfluidic systems. The balance of forces due to hydrodynamic resistance, channel pressure, and gravity determine flow rates and profiles in microfluidic devices. Assuming an incompressible, unidirectional, and Newtonian microfluid flow, the Navier-Stokes equation can be simplified below in equation (2) where $\rho \frac{\partial \vec{u}}{\partial t}$ is fluid convection force, $\eta \nabla^2 \vec{u}$ is the viscous force of the fluid, and $\nabla \vec{p}$ is the channel pressure gradient. The balance between these forces and laminar flow is a key principle when designing these microsystems[4].

$$\rho \frac{\partial \vec{u}}{\partial t} = \eta \nabla^2 \vec{u} - \nabla \vec{p} \qquad (2)$$

The ability to direct fluid flow at this scale allows for the control of a diffusional gradient between the interface of a fluidic channel and porous material. Such a gradient could be utilized

to deliver spatiotemporal cues to a 3D cell culture mimicking *in vivo* conditions. This platform would allow scientists and engineers to study different cellular pathophysiologies accurately as *in vitro* models of human tissue for optimizing cues and screening drugs.

Glioma

U87 cells are a human-derived glioblastoma cancer cell line. These cells are highly competitive in brain tissue which leads to successful infiltration and tumorigenesis[5]. Due to these phenotypes, gliomas have a high recurrence post-surgical removal. The traditional method of treatment comes in the form of radiosurgery and temozolomide[6]. While this can be effective in slowing the progression of the disease, the outlook of patients with high-grade glioblastoma multiforme (GBM) is grim. The 10-year survival rate of patients with this diagnosis is under 1%[7]. Novel therapeutic techniques are required to extend the survivability and quality of life of patients with high-grade gliomas.

GBM cells have a high affinity for chemotaxis in their environment. Finding a drug or chemoattractant that can control the movement of these cells would be extremely time-consuming. It is also difficult to recapitulate the biomechanical properties of brain tissue with current methods. This study proposes an open microfluidic platform design to study the cellular transformations under different drugs or chemo-attractants. A hydrogel-based 3D cell culture will be utilized to simulate the tissue environment. U87 GBM cells will be laden within the hydrogel to observe the effects of stimulation. Fig 1 shows a schematic of the proposed method and mechanism of cellular experiments. Success with this platform would allow future physicians the option of inducing *in situ* chemotaxis of GBM cells to “suck” the remaining malignant and dangerous cells out of the brain. Biocompatible patches or hydrogels laden with the specified drug could be placed directly

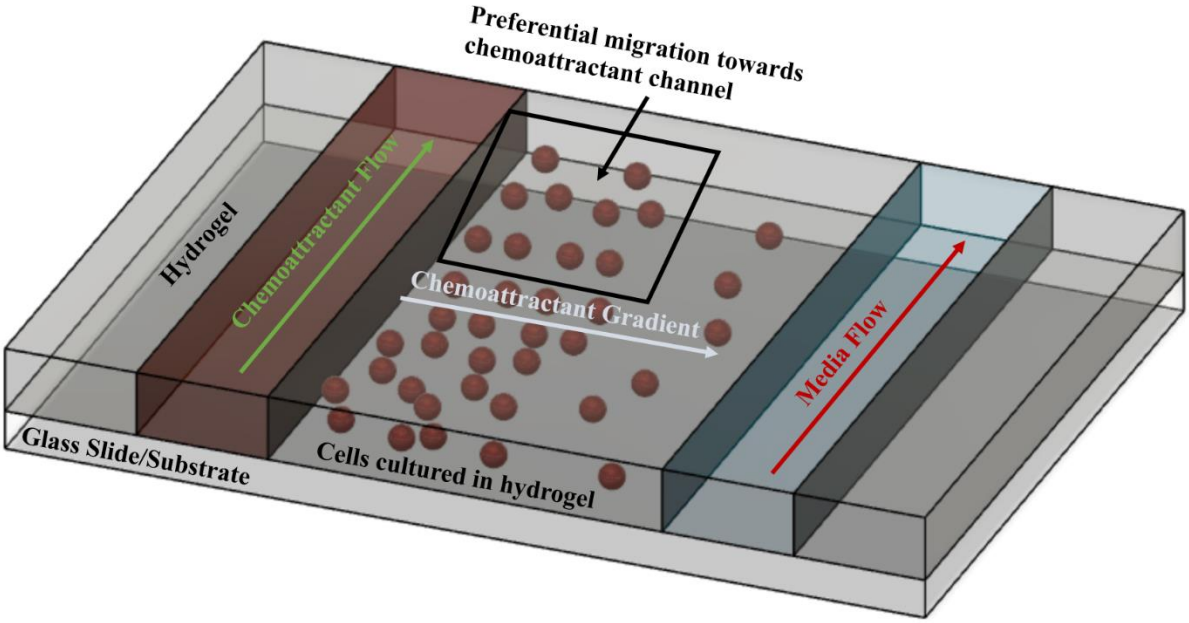

Figure 1. Three-dimensional schematic of the proposed open microsystem. Two opposite fluidic channels create a gradient through the central width of hydrogel causing cellular chemotaxis and signaling.

on brain tissue after surgical removal of the tumor. After removal of the implant, the leftover cells would be embedded, and the patient would be mutant-type cell free.

3D Cell Culture Techniques

Many recent studies have shown that three-dimensionally cultured cells exhibit higher levels of physiologically relevant behavior than their monoculture counterparts. Cells within *in vivo* conditions interact with neighboring cells and the shared extracellular matrix (ECM). Replicating the ECM-cell environment is imperative to the success of cell culture models[8]. Hydrogels have become a popular choice for 3D cell culture structures due to their mechanical, biocompatibility, and biochemical properties. A hydrogel must have adequate mechanical strength for suspension, attachment, and tissue formation after being laden with cells[9]. Combining microfabrication techniques and microfluidic flow control with hydrogel-based 3D cell cultures is a promising application to simulate biomimetic properties and conditions outside of the body.

Closed microfluidic systems enable optimal control of flow and diffusional profiles to create cues to cells under cultures. However, 3D cell culture requires 3D cell-laden hydrogels over millimeter-scale depths, which is hard to maintain in closed microsystems[10]. The thicker PDMS backing layer that is needed for fluidics and to mechanically support the hydrogel layer of millimeter-scale thickness leads to poorer gas permeability, thereby causing instabilities in pH and

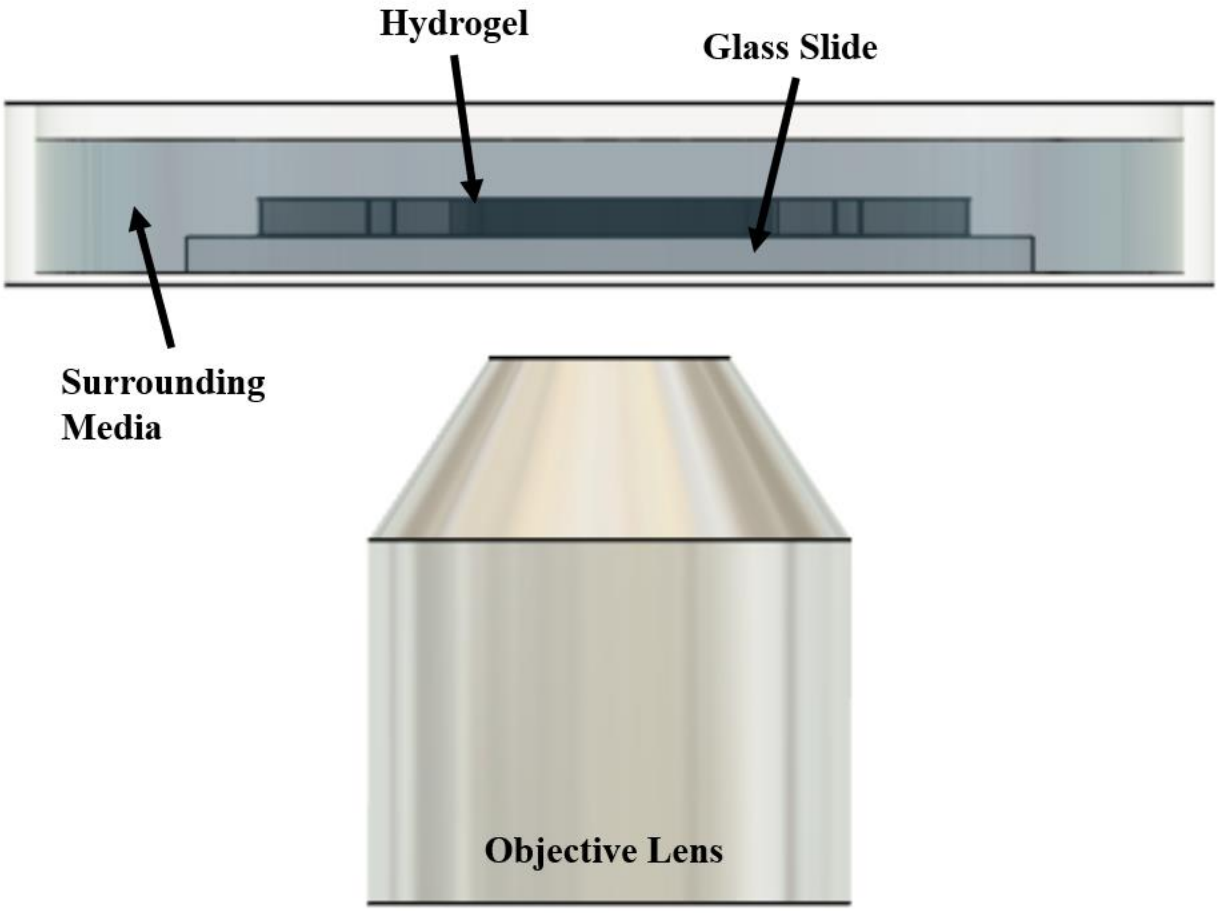

Figure 2. Side view of 3D cell culture technique. The hydrogel sits on top of a glass slide or well plate and is surrounded by media. An objective lens images through the culture from below.

temperature of the cell culture, as well as poor humidity control that can degrade the hydrogel. Access to nutrients and clearance of waste over extended culture periods is also poor in closed microfluidic systems. 3D culture in cell-laden hydrogels can proceed well in open-top systems[11],

but the integration of fluidic control to create gradients that provide chemotactic cues to direct cell migration is challenging.

Fig 2 shows the proposed method for 3D cell culturing. A cell-laden hydrogel will be crosslinked onto the surface of a glass slide or well plate. It must be surrounded with media to prevent structure shrinkage and cell death. The culture will be imaged from below using an inverted microscope similar to conventional imaging of cultures.

Chemical Gradient Formation and Control

Gradients drive many biological processes within the complex and dynamic environment of living tissue. These include cellular growth, migration, differentiation, inflammation, and cancer metastasis[12]. Biomaterials, such as hydrogels, have been used for many years to simulate chemotactic gradients to direct cell growth, differentiation, and migration[13]. But, traditional methods for gradient generation within large-volume hydrogel systems utilize passive, or static, methods[14]. Open microfluidics can address the challenge of dynamic gradient control through a millimeter-scale hydrogel.

A fluid flow containing a certain chemoattractant can diffuse through a porous material. Hydrogels' porosity allows for diffusional patterns to form[15]. A change in concentration involves both diffusion and convection. The scalar transport equation shown below (equation (3)) dictates the spatiotemporal profile of a chemical species within a system due to both physical phenomena, where c is the chemical species of interest, D is the diffusivity, v is the velocity field, and R describes sources or sinks of the species[16].

$$\frac{\partial c}{\partial t} = \nabla \cdot (D\nabla c) - \nabla \cdot (vc) + R \qquad (3)$$

The three equations described above are important to the design and implementation of a microfluidic system. While each part of the system can be understood, integration is a challenging

endeavor. This work combines open microfluidics with 3D hydrogel-based cell culturing to study the effects of spatiotemporal chemotactic cues from a dynamically controlled gradient on cell signaling and viability.

Chapter 2: System Design and Integration

Hydrogel Fabrication

This combined system brings individual components together to complete gradient formation. The first step of this process is hydrogel microfabrication. Past work has shown the effectiveness of injectable photocrosslinking[17]. A positive 3D-printed mold, fig 3, is used to create a negative polydimethylsiloxane (PDMS) microchannel (~1mm depth).

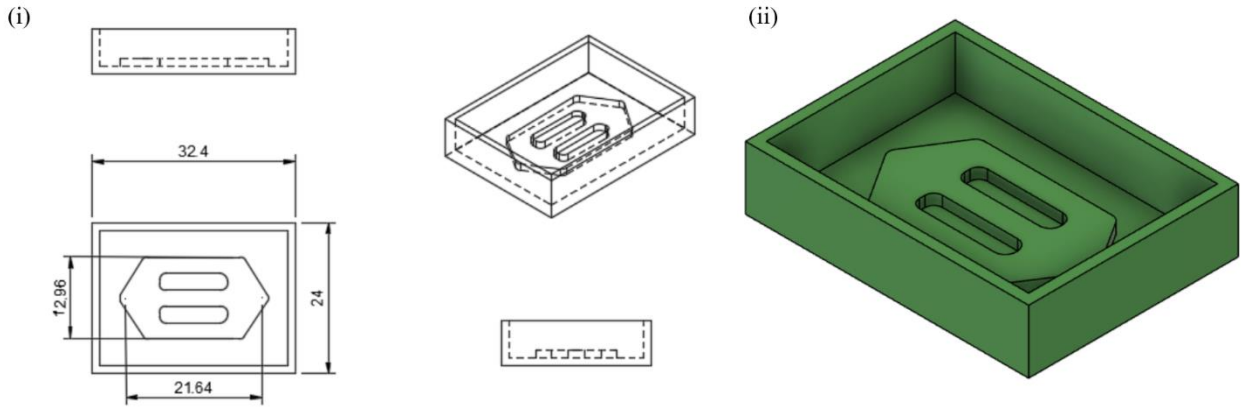

Figure 3. Schematics of 3D printed mold for PDMS injection. (i) Various views of designed mold and dimensions in mm. (ii) An example of a cured and printed mold ready for PDMS injection.

To pattern the cell-laden hydrogel layer with adjoining fluidic channels shown in Fig 4, a silanized glass coverslip is reversibly bonded with the PDMS microchannel into which the cell sample with hydrogel (composition and mechanics discussed below) is filled and UV crosslinked. Following crosslinking, the PDMS channel is released to leave a patterned cell-laden hydrogel layer with open areas for the adjoining fluidic channel used to create the chemotactic gradient. An image of this patterned hydrogel with the adjoining channel is also shown in Fig 4. The hydrogel is surrounded with culture media to enable nutrient delivery and ensure adequate hydration for 3D culture over 1 – 2 days.

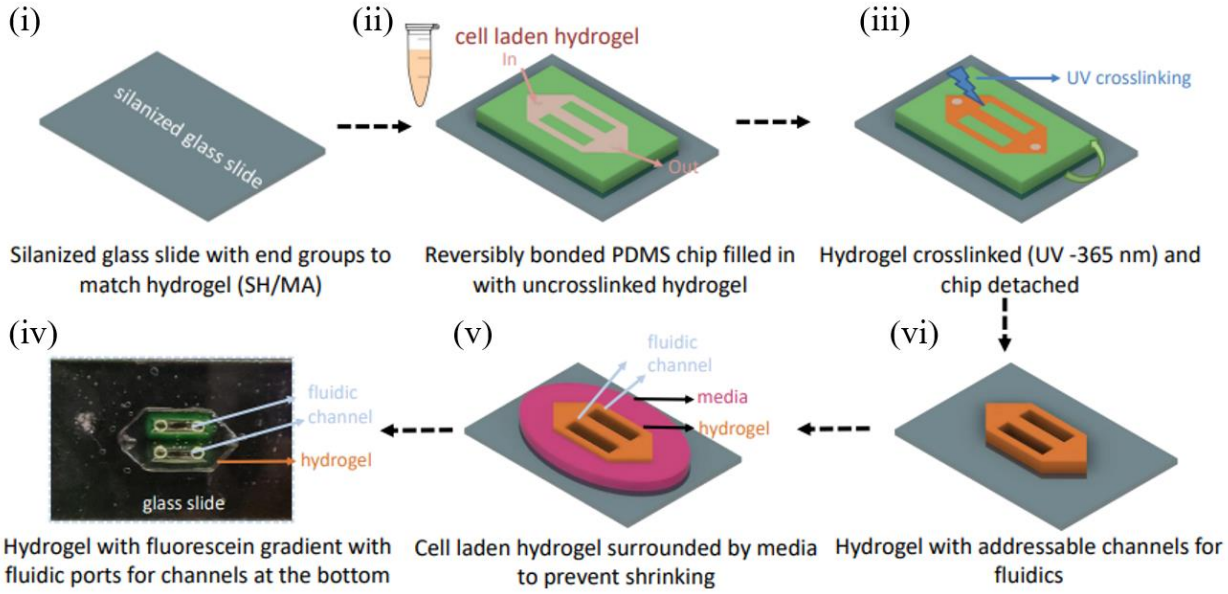

Figure 4. Patterning steps to fabricate individual hydrogel environments. (i) The glass must be silanized for adhesion to the crosslinked hydrogel. (ii) The PDMS mold is bonded to the glass and filled with the cell-laden hydrogel mixture. (iii) Photo-crosslinking solidifies the hydrogel in place on the glass slide. (vi) The PDMS mold is removed, and the hydrogel remains. (v) The structure is surrounded with media to prevent shrinking and cell death. (vi) An example of the fabricated hydrogel with addressable open fluidic channels.

Fluidic Control

Fluidic integration to deliver the chemoattractant along one side channel and culture media along the other side channel is accomplished using positive pressure on one side and a vacuum pump for negative pressure on the other side, thereby setting up gradient cues across the hydrogel width. A representation of this system can be seen in Fig 5 (i). A 3D-printed holder is used to

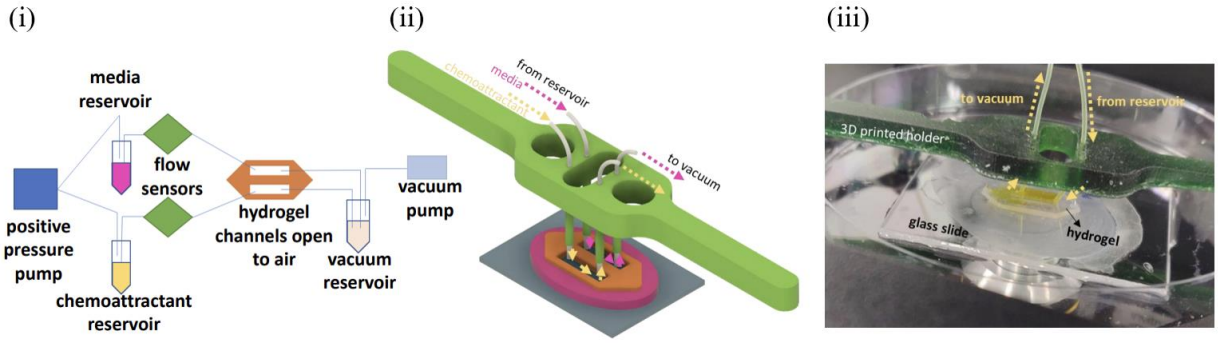

Figure 5. Microfluidic integration with the fabricated hydrogel structure. (i) Schematic of pump setup. (ii) Schematic of 3D printed holder and patterned hydrogel. (iii) Image of patterned GelMA hydrogel with tubing setup through the 3D printed holder, channel filled with yellow dye.

assemble the fluidic connections and maintain the outlet tubing to vacuum at a higher position than the incoming flow meniscus so that the side channels always remain filled and only the excess fluid is drawn from the input reservoir. Fig 5 (ii) shows a model of this integration and Fig 5 (iii) displays the integrated holder, fluidics, and hydrogel.

Live Image Data Acquisition

The final step of combining all parts is the utilization of the EVOS M7000 live-cell imaging microscope. This microscope houses an on-stage incubator to conduct long-term cell experiments. Fluidic interfaces within the environmental control connection allow for the addition of tubing from the pumps with the entire system. Images and z-stacks can be taken at different time points and used to recreate a timeline of events. Fluorescent and brightfield channels are utilized to characterize the chemotactic gradient, cell viability, and cell signaling and migration within the hydrogel.

Chapter 3: Biomechanical Recapitulation and Cell Viability

Hydrogel Formulation Optimization

The composition of the hydrogel must be compatible with our photo-crosslinking technique and the cell line in interest. Hyaluronic acid (HA) hydrogels allow the mimicking and incorporation of brain tissue biomechanical properties into the 3D culture system[18]. U87 glioblastoma cells have high viability within a HA hydrogel culture. But, HA does not contain RGD peptide groups that are necessary for cell migration and proliferation[19]. U87 cells have lower viability in gelatin methacrylate (GelMA). But, this hydrogel base provides the necessary RGD peptides[20]. Table 1 shows the key differences between these gel bases. These bases on their own will not create the necessary environment to allow for U87 growth, signaling, and proliferation. Norbornene-modified HA (NorHA) and GelMA must be combined to allow for cell functionality in the hydrogel.

Formulation	1% NorHA	10% GelMA
Stiffness	0.5-3 kPa	35 kPa
Viability (36 h)	90%	60%
Migration	No RGD groups	Has RGD groups

Table 1. Creating the hydrogel structure with only GelMA or NorHA gives it different properties. NorHA recapitulates the stiffness and viability of brain tissue, but it does not provide RGD groups necessary for migration. GelMA can provide the hydrogel with these necessary RGD groups.

LAP is a photo-initiator that is needed for the crosslinking of GelMA and NorHA. Dithiothreitol (DTT) is also needed to reduce the free disulfide bonds in NorHA to complete crosslinking. Both chemical structures change after photo-treatment and can be seen below in Fig 6 (i) and Fig 6 (ii). When in combination, the hydrogel must be formulated with both LAP and DTT. 1X Phosphate-buffered saline (PBS) is laden with cells or added on its own depending on the type of experiment being conducted with the hydrogel. GelMA, NorHA, LAP, DTT, and PBS

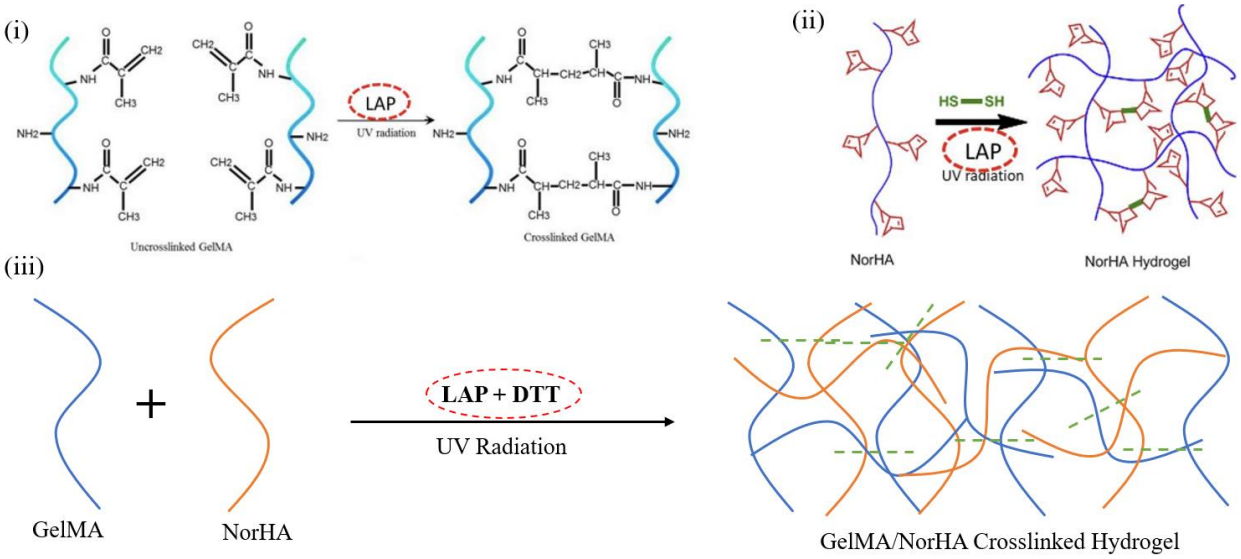

Figure 6. Individual and hybrid hydrogel configurations. (i) Molecular structure of gelatin methacrylate before and after crosslinking. (ii) Molecular structure of norbornene modified hyaluronic acid before and after crosslinking. (iii) Structure of GelMA/NorHA hybrid hydrogel before and after crosslinking.

are mixed with proper proportions to crosslink the hybrid gel structure. Fig 6 (iii) shows the formation of the hybrid hydrogel due to crosslinking.

Brain tissue has an average stiffness of 1389 Pa for white matter to 1895 Pa for gray matter[21]. It is important to simulate this biomechanical property to allow for the cells to effectively

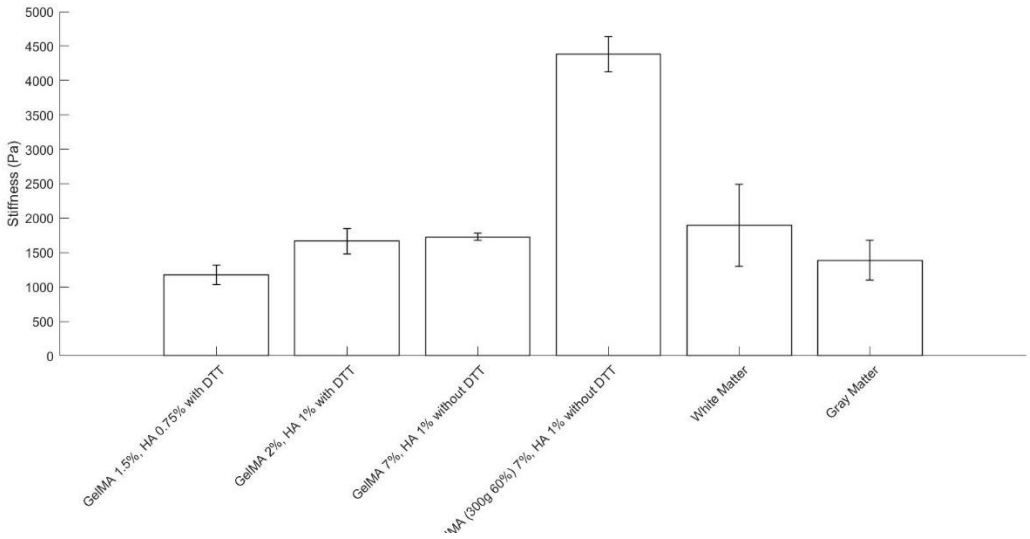

Figure 7. Youngs' modulus of hydrogel formulations compared to that of brain tissue. GelMA 2%, HA 1% with DTT and GelMA 7%, HA 1% without DTT recapitulate the measured stiffness of white and gray matter.

grow and change in their environment. The formulation of the hydrogel was varied and optimized to find the composition that would have the same level of thickness. A nanoindenter was used to measure the effective Youngs' modulus of each hydrogel structure and compared it to that of brain tissue, Fig 7. Both the second and third formulations of the hydrogel composition recapitulate the stiffness of brain tissue accurately. GelMA 2%, HA 1% with DTT was chosen as the composition to integrate with the entire system.

Cell Viability Post Fluidic Control

The viability of U87 cells within the hydrogel was quantified with fluorescence imaging after the 24-hour culture experiment. In addition, cell division, movement, and migration were tracked

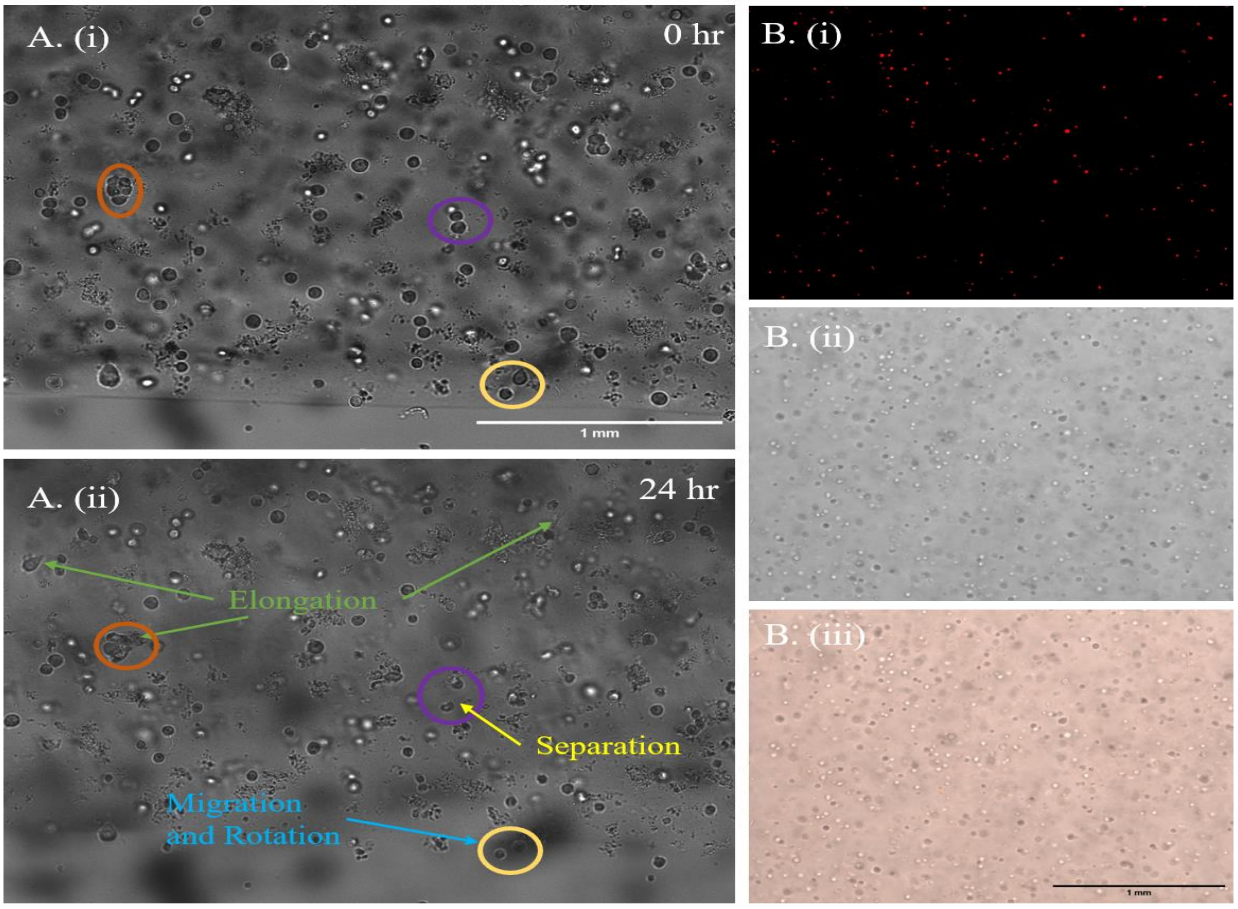

Figure 8. Cell viability within the hydrogel structure integrated with the fluidic system. A. Cell movement, division, and morphology changes over the 24-hour period. (i) Time = 0 hours. (ii) Time = 24 hours. B. Fluorescent (i), brightfield (ii), and overlay (iii) of cell staining with propidium iodide to quantify survivability over the experiment period.

during the entire time of each experiment using brightfield imaging. Fig 8 A. shows these changes from the initial time point (i) to the end of the experiment (ii). Fig 8 B. displays the fluorescent staining with propidium iodide used to quantify cell viability through the hydrogel (i), the same brightfield image (ii), and the merged channel image (iii). Fluorescing cells are no longer viable and were counted against the total cell composition in each image. Cell viability percentages ranged from 50 – 80% averaging 71±3.4%. Along with the confirmation of cell division and random migration throughout the hydrogel, it can be concluded that these hydrogels are suitable environments to use in our integrated microsystem.

Chapter 4: Chemoattractant Gradient Formation and Cellular Response

Characterization of Chemical Gradient from Hydrogel/Channel Boundary

Once the hydrogel has been fabricated and integrated with the system, timelapse image data is taken over the experiment period. The gradient formed between the channels was first characterized without cells. Brightfield image data was overlayed with fluorescence through the GFP 482nm/524nm filter from the EVOS. One fluidic channel was perfused with 1X PBS and the second channel with FITC-dextran in 1X PBS. Flow rates of 7.5 µl/min were used in both channels. Z-stacks were taken through multiple sections of the hydrogel and fluorescent channel boundary. ImageJ was utilized to analyze fluorescent intensity through the hydrogel. With a known channel concentration of 0.33 mg/ml, the intensity was normalized and correlated with concentration values. FITC-dextran with molecular weights of 400 Da and 10000 Da were tested. The results of

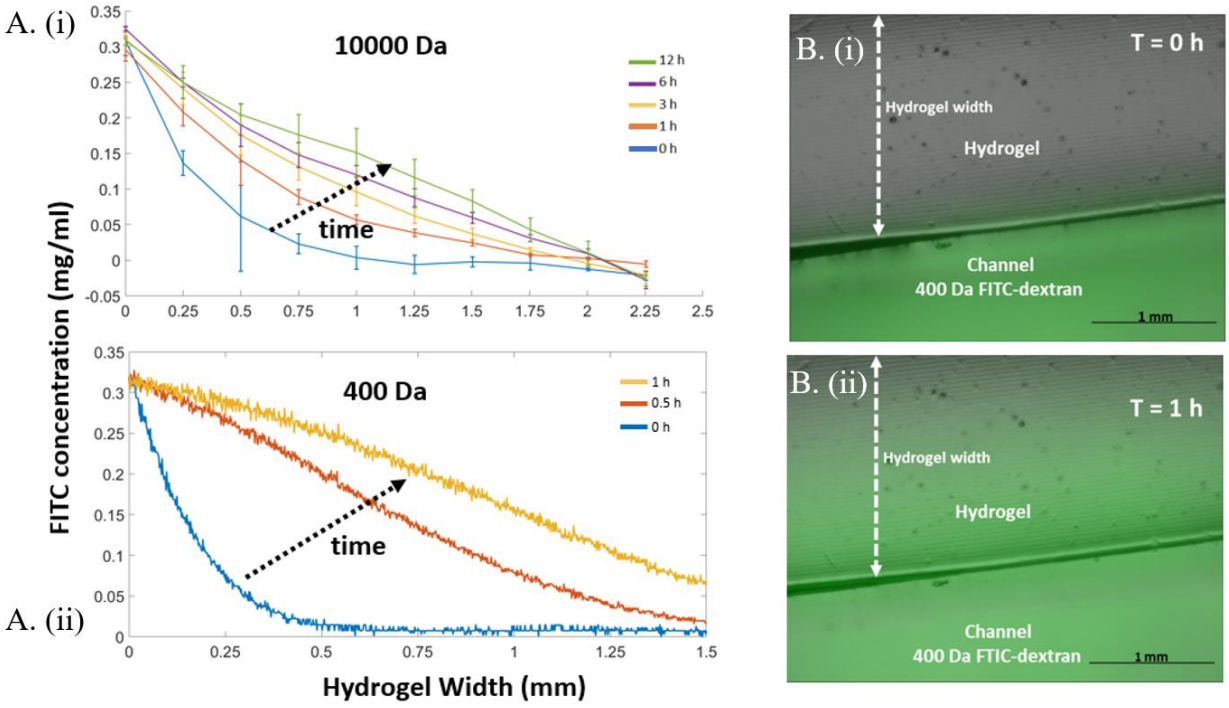

Figure 9. A. Temporal development of gradient across the open hydrogel. (i) 10000 Da FITC dextran, gradient develops slowly over 12 hrs, (ii) 400 Da FITC dextran, gradient develops rapidly to approach steady state within 1 hr. B. Brightfield and FITC overlay of emerging gradient across the hydrogel at two timepoints using 400 Da FITC dextran: (i) 0 hr, (ii) 1 hr.

the gradient formation can be seen in Fig 9 A.(i) and Fig 9 A.(ii). The 400 Da FITC-dextran took much less time to reach a steady-state concentration. Fig 9 B.(i) and Fig 9 B.(ii) show examples of brightfield and fluorescent overlays used to quantify the gradient through the hydrogel.

Larger molecular weight molecules have higher molecular radii. Diffusivity is inversely affected by molecular radius. Equation (4) below is the Stokes-Einstein equation that expresses this relationship, where D is diffusivity, k_b is the Boltzmann constant, T is the absolute temperature, r is the spherical molecular radius, and η_0 is the solvent viscosity[22]. An increase in molecular

$$D = \frac{k_b T}{6\pi r \eta_0} \qquad (4)$$

weight results in a proportional decrease in diffusivity. Relating this change to equation (3), it can be surmised that a change in diffusivity directly affects the change in concentration. As the molecular weight of the FITC-dextran increased, the time it took the gradient to reach steady-state increased due to a lower diffusivity and change in concentration. This confirms the validity of the micropatterned gradient and our fluidic generation technique. In addition, we can predict the diffusional profile of CXCL12, our chemoattractant of interest, due to its almost equal molecular weight to 10000 Da FITC-dextran.

Cellular Response to Chemoattractant

U87 cells have a high density of surface membrane proteins that bind preferentially to chemo-attractants. One such membrane protein is chemokine receptor 4 (CXCR4). CXCR4/CXCL12 interactions are crucial in the roles of tumor physiology[23]. CXCL12 triggers calcium mobilization into the cell[24]. An increase in intracellular calcium has been shown to promote migration through membrane polarization and stretch-mediated proteins[25,26]. Therefore, stimulation with CXCL12 should increase intracellular calcium concentration. To verify that stimulation occurs and to further characterize the gradient, fluorescent staining of the cells was

accomplished with Fluo-4 AM. This cell-permeant has an excitation/emission of 494nm/506nm in its Ca^{2+}-bound form. Image acquisition was taken on the EVOS M7000 microscope with the same GFP filter cube. There is sufficient spectral overlap to accurately measure the fluorescent signal from the permeant.

Verification of direct CXCL12 stimulation was performed. U87 cells were incubated in a polystyrene well-plate and treated appropriately with the permeant. An experiment was conducted to measure the fluorescent intensities before and after stimulation. A CXCL12 concentration of 100ng/ml was added after 15 minutes. Fig 10 A. shows the fold increase of fluorescence after stimulation at 15 minutes. Fig 10 B. displays an example of fluorescent U87 cells (i), the brightfield image channel (ii), and the merged image (iii).

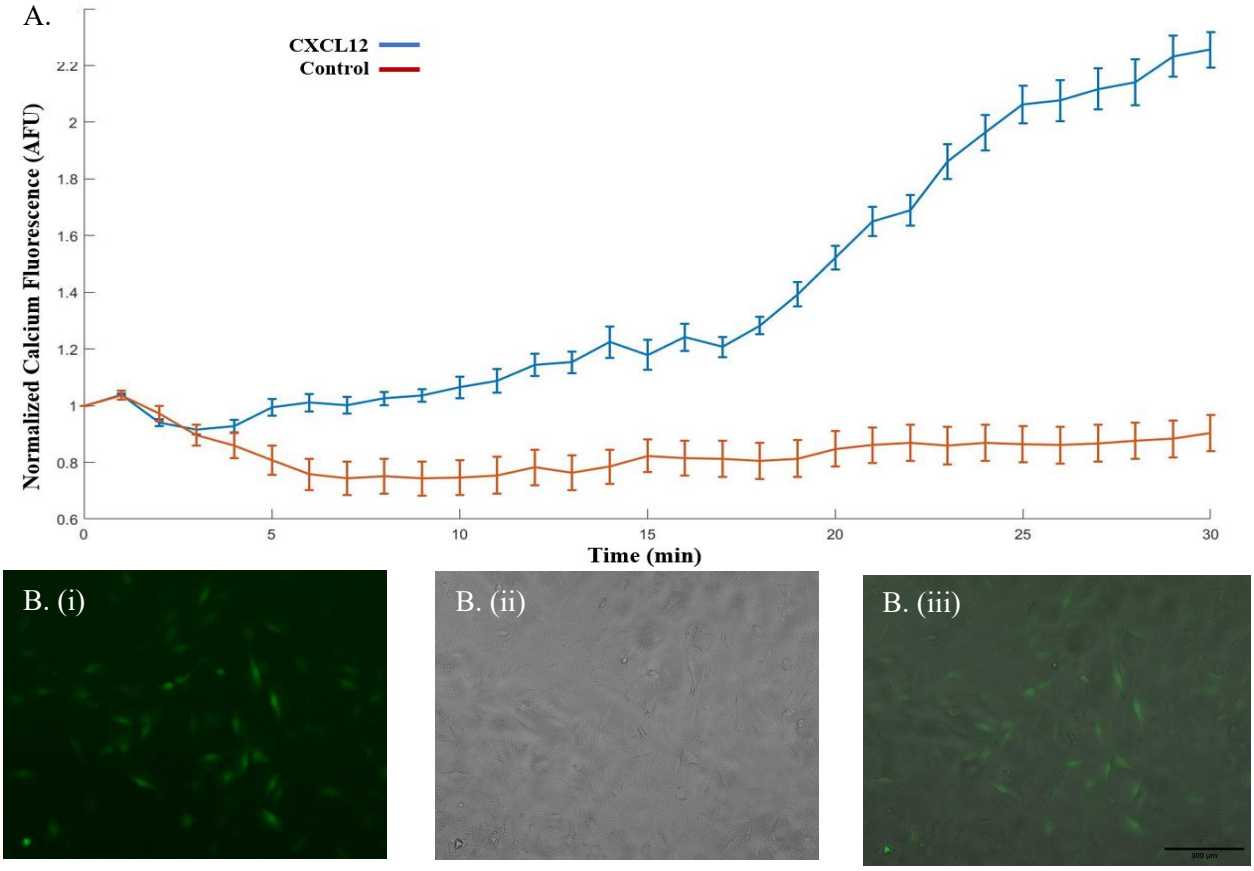

Figure 10. Direct stimulation of U87 cells on a monoculture well plate. A. Treatment occurred at 15 minutes and the fold increase of fluorescence was observed versus the control group. B. Fluorescent (i), brightfield (ii), and merged (iii) images of monocultured cells.

Fluorescence intensities were measured from individual cells at known distances from the hydrogel/channel boundary. The fluidic control was performed with 1X MEM in one channel and 66.7 ng/ml of CXCL12 within 1X MEM in the other channel. Flow rates of 7.5 µl/min were also used in both channels to create a similar gradient to the 10000 Da FITC-dextran. Fig 11 (i) displays the fluorescent signal during four hours of gradient generation. Fig 11 (ii) shows an example of image data used to quantify fluorescent intensities. The cells in the CXCL12-treated group

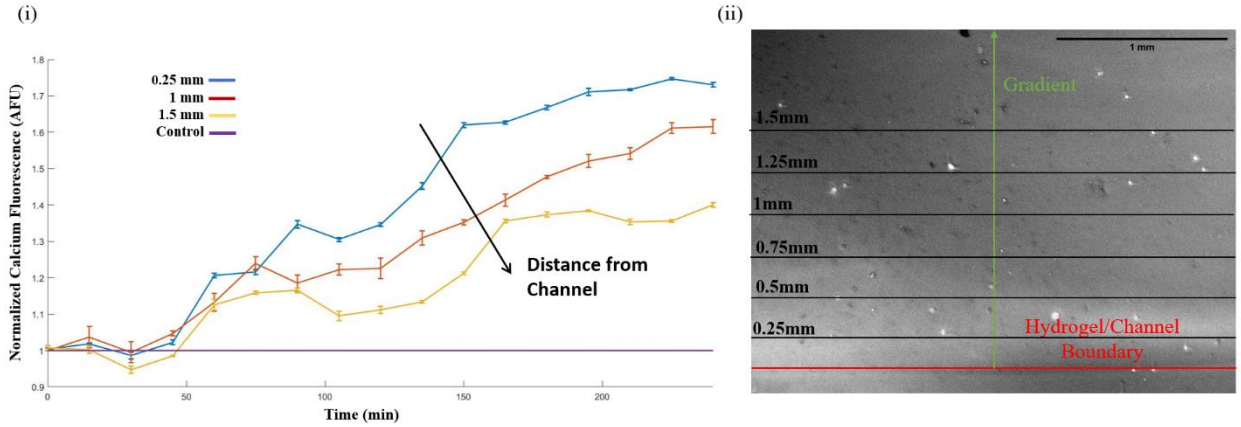

Figure 11. Fluorescent signal gradient through hydrogel width. (i) Normalized arbitrary fluorescence units of cells within the hydrogel. Cells were measured at increasing distances from the hydrogel/channel boundary from time 0 – 4 hrs. Cells in the control group were measured and averaged through the entire width of the hydrogel. (ii) An example of a fluorescent cell image used for data analysis. The gradient forms towards the top of the image from the hydrogel/channel boundary.

increased in intensity around 45-60 minutes after initial gradient generation and eventually reached varying levels of steady-state signal increase. There is a correlation between this increase and the distance from the hydrogel/channel boundary. Cells closer to the channel had higher signal intensities than those further from the boundary. No correlation between the control and distance into the hydrogel was observed.

Migration

Brightfield images of the hydrogel/channel boundary were taken every 30 minutes within 24 hours. Cell densities were measured at 0, 12, and 24 hours to measure the quantification of

migration. Fig 12 A. displays the difference between CXCL12-stimulated cells and the control group. Fig 12 B. shows example cells moving within the hydrogel at 0 (i), 6 (ii), and 12 (iii) hours. While cells did move towards the channel with chemoattractant, some still exhibited random movement.

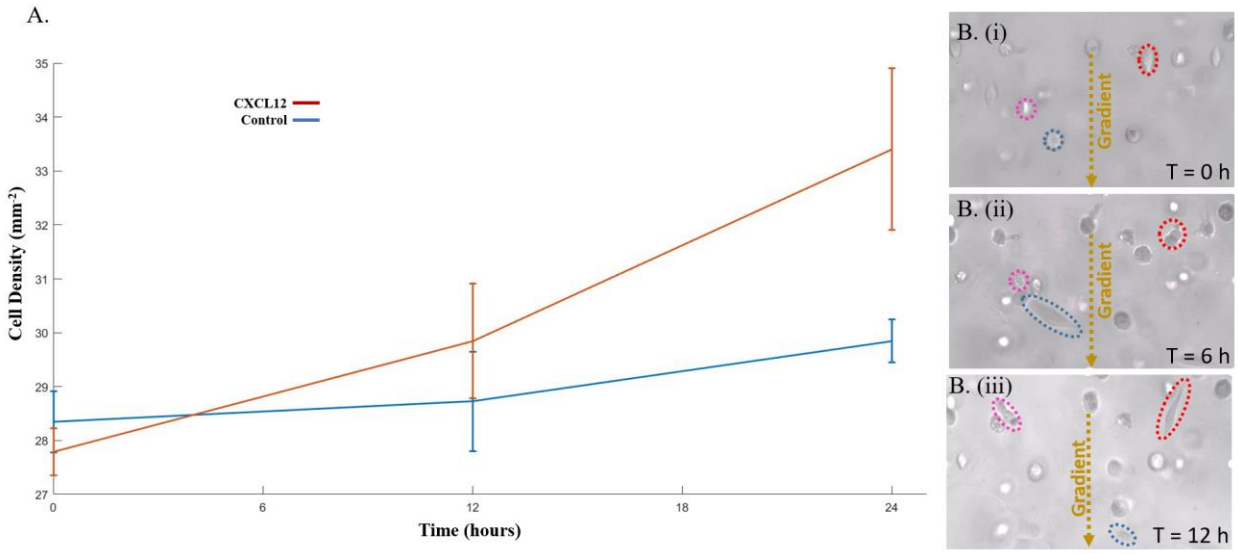

Figure 12. Characterization of U87 migration. A. Cell densities near the hydrogel/channel were measured at 0, 12, and 24 hours. B. Brightfield images showing the movement of selected cells at 0 (i), 6 (ii), and 12 (iii) hours. The concentration gradient is occurring from the top of the image where the channel is located.

Chapter 5: Conclusion and Future Improvements

Novel fabrication, integration, and dynamic generation of a chemotactic gradient through a hydrogel was explored in this study. An open microfluidic system was created through a positive-negative-positive photo-crosslinking process. The crosslinked composite hydrogel 3D cell culture was integrated with a designed pressure and flow control fluidics system. An EVOS M7000 microscope with an on-stage incubator was used to capture image data for the necessary quantification of gradient formation and cellular response. U87 glioblastoma cells were utilized as the model cell line to test cellular viability and proliferation potential. These components combined to create the microsystem used in this study.

Fluorescent signal intensities were used to characterize the gradient formation across the channel/hydrogel boundary and the cellular response to the chemoattractant. The gradient formation was dependent on the molecular weight of the solute introduced into the open channel. While the flow rates of both channels were kept the same throughout, varying the channel flow rates would alter the gradient. This is allowed by the inertial component in equation (3) and indicates the dynamic abilities of this microsystem. 10000 Da FITC-dextran was shown to reach a steady state through the hydrogel at 12hrs after the experiment began. It can be assumed that CXCL12 would reach this steady state within similar periods due to their very close molecular weights. The chemoattractant created a significant fold increase in calcium signaling after direct stimulation, as measured by fluorescence. In addition, the 3D-cultured cellular response did show a correlation between distance from the channel and fluorescent fold increase normalized to the control over the course of the stimulation. Migration in the hydrogel structures did occur. The cell densities of the stimulated cells at the hydrogel/channel boundary increased at a higher rate than that of the control group. While the absolute change occurred, mechanisms such as cell division,

random migration, and movement in the Z-axis can affect the results. More investigation is necessary to attribute the increase in cell density to migration due to chemoattractant stimulation.

There were multiple problems to overcome throughout the lifetime of this project. Some obstacles can be improved upon in future iterations of this study. Even within a clean BSL-2 laboratory space, sterility was extremely difficult. Integrated microsystem experiments could not be continuously run after 24-36 hours due to heavy contamination within the cell culture. This is due to not being able to sterilize every component used for hydrogel fabrication and the inability to perform the experiments completely in a biohood. Studies conducted up to 48-72 hours would need better decontamination protocols. Flow control with the fluidic system was cumbersome to set up. A completely custom and centralized system might reduce the complexity associated with using multiple pressure sources for various pumps. Better flow control would improve the experiment's reproducibility in the future. In addition, the media being perfused into the channels was not kept at the same environmental conditions as the cells within the on-stage incubator. While media and chemoattractant were slowly refreshed, the system had to continuously work to keep the environmental conditions at the appropriate values. This can be improved in later platform designs for studying biomimetic recapitulation in 3D cell cultures. These problems could have been attributed to the lower amount of directed migration than expected. Solving them might be the key to moving forward.

While the project has its obvious obstacles, it shows great promise for the future of *in vitro* cell studies attempting to simulate tissue conditions. Forthcoming research on its application in treating GBM will give diagnosed patients a better chance for survival. Not only does the dynamic ability of the gradient formation allow for an easier method to study drug and chemoattractant diffusion parameters in simulated tissue, but the hydrogel composition could also be modified to

use any cell line. We plan to use this method to study the pathophysiologies of more cancer cell lines. Pancreatic ductal adenocarcinoma (PDAC) cells would be a great candidate to investigate the effect of shear stress on the generation of floating cells that simulate circulating tumor cells (CTCs) using a 3D cell culture. We hope this work inspires researchers and engineers to continue our work to better simulate and understand *in vivo* conditions for the creation of novel therapeutic approaches that can accurately and precisely treat human diseases.

References

1. Whitesides, G. M. The origins and the future of microfluidics. *Nature* **442**, 368–373 (2006).
2. Faustino, V., Catarino, S. O., Lima, R. & Minas, G. Biomedical microfluidic devices by using low-cost fabrication techniques: A review. *Journal of Biomechanics* **49**, 2280–2292 (2016).
3. Convery, N. & Gadegaard, N. 30 years of microfluidics. *Micro and Nano Engineering* **2**, 76–91 (2019).
4. Bahrami, M., Yovanovich, M. M. & Culham, J. R. Pressure Drop of Fully-Developed, Laminar Flow in Microchannels of Arbitrary Cross-Section. *Journal of Fluids Engineering* **128**, 1036–1044 (2006).
5. Kundu, P., Santosh, V. & Kondaiah, P. Mechanisms of cell competition in glioblastoma: A narrative review. *Glioma* **3**, 154 (2020).
6. Radiosurgery reirradiation for high-grade glioma recurrence: a retrospective analysis | SpringerLink. https://link.springer.com/article/10.1007/s10072-015-2172-7.
7. Jovčevska, I. Genetic secrets of long-term glioblastoma survivors. *Bosn J Basic Med Sci* **19**, 116–124 (2019).
8. Lee, S. H., Shim, K. Y., Kim, B. & Sung, J. H. Hydrogel-based three-dimensional cell culture for organ-on-a-chip applications. *Biotechnology Progress* **33**, 580–589 (2017).
9. Zhu, J. & Marchant, R. E. Design properties of hydrogel tissue-engineering scaffolds. *Expert Review of Medical Devices* **8**, 607–626 (2011).
10. Varma, S. & Voldman, J. Caring for cells in microsystems: principles and practices of cell-safe device design and operation. *Lab Chip* **18**, 3333–3352 (2018).
11. Lee, U. N. *et al.* Layer-by-layer fabrication of 3D hydrogel structures using open microfluidics. *Lab Chip* **20**, 525–536 (2020).

12. Keenan, T. M. & Folch, A. Biomolecular gradients in cell culture systems. *Lab Chip* **8**, 10.1039/b711887b (2008).

13. Heit, B., Tavener, S., Raharjo, E. & Kubes, P. An intracellular signaling hierarchy determines the direction of migration in opposing chemotactic gradients. *J Cell Biol* **159**, 91–102 (2002).

14. Jo, H., Yoon, M., Gajendiran, M. & Kim, K. Recent Strategies in Fabrication of Gradient Hydrogels for Tissue Engineering Applications. *Macromolecular Bioscience* **20**, 1900300 (2020).

15. Dravid, A. *et al.* A Macroscopic Diffusion-Based Gradient Generator to Establish Concentration Gradients of Soluble Molecules Within Hydrogel Scaffolds for Cell Culture. *Frontiers in Chemistry* **7**, (2019).

16. Jr, C. E. B., Gershtein, V. & Li, X. J. *Computational Fluid Dynamics in Industrial Combustion*. (CRC Press, 2000).

17. Khunmanee, S., Jeong, Y. & Park, H. Crosslinking method of hyaluronic-based hydrogel for biomedical applications. *J Tissue Eng* **8**, 2041731417726464 (2017).

18. Nakod, P. S., Kim, Y. & Rao, S. S. Three-dimensional biomimetic hyaluronic acid hydrogels to investigate glioblastoma stem cell behaviors. *Biotechnol Bioeng* **117**, 511–522 (2020).

19. Cai, Z. *et al.* Capturing dynamic biological signals via bio-mimicking hydrogel for precise remodeling of soft tissue. *Bioactive Materials* **6**, 4506–4516 (2021).

20. Bupphathong, S. *et al.* Gelatin Methacrylate Hydrogel for Tissue Engineering Applications—A Review on Material Modifications. *Pharmaceuticals (Basel)* **15**, 171 (2022).

21. Budday, S. *et al.* Mechanical properties of gray and white matter brain tissue by indentation. *Journal of the Mechanical Behavior of Biomedical Materials* **46**, 318–330 (2015).

22. Miyamoto, S. & Shimono, K. Molecular Modeling to Estimate the Diffusion Coefficients of Drugs and Other Small Molecules. *Molecules* **25**, 5340 (2020).

23. Nimmagadda, S., Pullambhatla, M. & Pomper, M. G. Immunoimaging of CXCR4 expression in brain tumor xenografts using SPECT/CT. *J Nucl Med* **50**, 1124–1130 (2009).

24. Agle, K. A., Vongsa, R. A. & Dwinell, M. B. Calcium Mobilization Triggered by the Chemokine CXCL12 Regulates Migration in Wounded Intestinal Epithelial Monolayers. *J Biol Chem* **285**, 16066–16075 (2010).

25. Calcium signalling during chemotaxis - PubMed. https://pubmed.ncbi.nlm.nih.gov/7587614/.

26. Lee, J., Ishihara, A., Oxford, G., Johnson, B. & Jacobson, K. Regulation of cell movement is mediated by stretch-activated calcium channels. *Nature* **400**, 382–386 (1999).